PDIA3P1 Promotes Temozolomide Resistance in Glioblastoma by Inhibiting C/EBPβ Degradation to Facilitate Proneural-to- Mesenchymal Transition

Zijie Gao
Qilu Hospital of Shandong University
Jianye Xu
Qilu Hospital of Shandong University
Yang Fan
Qilu Hospital of Shandong University
Yanhua Qi
Qilu Hospital of Shandong University
Shaobo Wang
Qilu Hospital of Shandong University
Shulin Zhao
Qilu Hospital of Shandong University
Xing Guo
Qilu Hospital of Shandong University
Hao Xue
Qilu Hospital of Shandong University
Lin Deng
Qilu Hospital of Shandong University
Rongrong Zhao
Qilu Hospital of Shandong University
Chong Sun
Immune Regulation in Cancer, Germany Cancer Research Center
Ping Zhang
Qilu Hospital of Shandong University
Gang Li (dr.ligang@sdu.edu.cn)
Qilu Hospital of Shandong University

Research Article

Keywords: PDIA3P1, Temozolomide, Proneural-to-Mesenchymal Transition, Glioma Stem Cells, C/EBPβ, MDM2, Neflamapimod

Posted Date: April 5th, 2022

DOI: https://doi.org/10.21203/rs.3.rs-1509672/v1

Abstract

Background

Resistance to temozolomide (TMZ) is a major obstacle to prevention of recurrence after surgery for glioblastoma (GBM). Although long noncoding RNAs (lncRNAs) play wide roles in GBM, the lncRNAs that regulate TMZ resistance have not been elucidated clearly. This study aims to identify lncRNAs that may affect TMZ treatment sensitivity and to explore novel therapeutic strategies to overcome TMZ resistance in GBM.

Methods

The lncRNAs associated with TMZ resistance were explored based on Cancer Cell Line Encyclopedia (CCLE) dataset and Genomics of Drug Sensitivity in Cancer (GDSC) dataset. Quantitative real-time PCR (qRT-PRC) was used to detect the expression of PDIA3P1 in TMZ-resistant and TMZ-sensitive GBM cell lines. Both gain-of-function and loss-of-function studies were used to assess the effects of PDIA3P1 on TMZ resistance through in vitro and in vivo assays. Glioma Stem Cells (GSCs) were used to determine the effect of PDIA3P1 on GBM subtype. The hypothesis that PDIA3P1 promotes proneural-to-mesenchymal transition (PMT) was established by bioinformatics analysis and functional experiments. RNA pull-down and RNA immunoprecipitation (RIP) assays were performed to examine the interaction between PDIA3P1 and C/EBPβ. The post-translational modification mechanism of C/EBPβ was verified using ubiquitination and co-immunoprecipitation (co-IP) experiments. The CompuSyn was leveraged to calculate the combination index (CI) and the antitumor effect of TMZ with Neflamapimod (NEF) was validated both in vitro and in vivo.

Results

We identified a lncRNA, PDIA3P1, which was upregulated in TMZ-resistant GBM cell lines. Overexpression of PDIA3P1 promoted the acquisition of TMZ resistance, whereas knockdown of PDIA3P1 restored TMZ sensitivity. PDIA3P1 was upregulated in MES-GBM, promoted PMT progression in GSCs, and caused GBMs to be more resistant to TMZ treatment. Mechanistically, PDIA3P1 disrupted C/EBPβ-MDM2 complex and stabilized C/EBPβ protein by preventing it from MDM2-mediated ubiquitination. The expression of PDIA3P1 was up-regulated in a time- and a concentration-dependent manner after TMZ treatment. The TMZ-induced upregulation of PDIA3P1 was mediated by p38α-MAPK signaling pathway. NEF is a small molecule drug that specifically targets p38α with excellent blood-brain barrier (BBB) permeability. NEF could block TMZ-responsive PDIA3P1 upregulation and produced synergistic effects with TMZ at specific concentrations. The combination of TMZ and NEF exhibited excellent synergistic antitumor effects in vitro and in vivo.

Conclusions

PDIA3P1 promoted PMT through stabilization of C/EBPβ, thereby reducing the sensitivity of GBM cells to TMZ treatment. NEF could inhibit TMZ-responsive PDIA3P1 upregulation and NEF combined with TMZ

could provide better anti-tumor effects.

Introduction

Glioblastoma multiforme (GBM) is the most common malignant and aggressive tumor of the central nervous system[1, 2]. Almost all patients with GBM relapse despite the usual combination of surgery, chemotherapy and radiation therapy, and the median survival time is approximately 12 to 15 months for decades[3, 4]. The obstacles to glioma treatment are due not only to the limited extent of tumor that can be safely removed, but also to resistance to adjuvant therapy after surgical resection [5]. Temozolomide (TMZ), a second-generation oral alkylating agent, is the first-line chemotherapeutic agent for patients with GBM [6, 7]. However, almost all patients develop resistance to TMZ and relapse after a progression-free survival period of 7 to 10 months [8]. Therefore, it is urgent to elucidate the underlying mechanisms of TMZ resistance in order to treat and prevent the recurrence of GBM.

Long non-coding RNAs (LncRNAs) is a class of heterogeneous RNA that are more than 200 nucleotides in length and limited protein coding potential [9]. lncRNAs have been proved to perform diverse cellular functions, including transcriptional regulation in cis or trans, organization of nuclear domains, and post-transcriptional regulation by interacting with miRNAs, mRNAs, or proteins [10–12]. Emerging evidence showed that lncRNAs were associated with multiple features of cancer, such as proliferation, apoptosis, metastasis, metabolism, and therapy resistance, etc [13, 14]. Recent studies have demonstrated that lncRNAs regulate numerous signaling pathways through interactions with proteins [15–17]. However, the regulation of post-translational modifications by lncRNAs and the subsequent impact on TMZ treatment resistance in GBM remains largely ambiguous.

Various mechanisms contribute to TMZ resistance in GBM, of which, GBM cells heterogeneity and plasticity are thought to be key factors driving treatment resistance and tumor recurrence [18]. Based on bulk RNA sequencing findings, Intertumor heterogeneity is manifested by at least three GBM subtypes, including proneural (PN), classical (CL) and mesenchymal (MES) [19]. Heterogeneity is also manifested by differences in the developmental status of GBM cells in tumors. Glioma stem cells (GSC) are a group of cells with capacity for self-renewal and asymmetric differentiation [20]. The presence of GSCs is thought to be a driving force in tumorigenesis, tumor propagation and preferential resistance to radiotherapy and chemotherapy, and thus GSCs are considered a valuable model for studying GBM [21]. GBM of PN and MES subtypes correspond to PN and MES GSC, respectively, but no GSC corresponding to CL subtype of GBM have been identified [22]. Recent studies have shown that the subtype of GBM will undergo a transition from PN to MES (PMT) type as the disease progresses and the tumor recurs [23–25]. PMT is therefore considered to be a marker of tumor tolerance against multiple treatments and recurrence. A variety of possible mechanisms drive the occurrence of PMT, including intracellular signaling pathways and extracellular tumor microenvironment (TME). For instance, Carro et al. identified that STAT3 and C/EBPβ as the two master regulators (MRs) of PMT [26]. In addition, the impact of treatment and the subsequent selective pressure within the tumor may also contribute PMT [27]. However, the mechanisms of treatment-induced PMT and modulation of MRs by lncRNAs remain unclear.

In this study, we identified a key LncRNA, PDIA3P1, which is closely associated with GBM TMZ therapy resistance and recurrence. Previous in vitro and vivo assays showed that knockdown of PDIA3P1 resulted in decreased resistance to TMZ in glioma cells; in contrast, overexpression of PDIA3P1 resulted in higher resistance of glioma cells to TMZ. Mechanically, PDIA3P1 promoted PMT by stabilizing CEBPβ, thereby enabling GSCs to acquire preferential resistance to TMZ treatment. Even more valuable was that we identified a drug named Neflamapimod (NEF), a specifically targeted drug against p38α that has the ability to easily cross the blood-brain barrier (BBB). We demonstrated that NEF could inhibit TMZ-induced upregulation of PDIA3P1 and enhanced the sensitivity of glioma cells to TMZ treatment.

Materials And Methods

Public data collection

TMZ sensitivity data from GBM cell lines were obtained from the GDSC (www.cancerRxgene.org) database which is the largest public database on molecular markers of cancer drug sensitivity and drug response[28]. Corresponding cell lines expression data were available from the CCLE (https://portals.broadinstitute.org/ccle/) [29]. Transcript level data, somatic mutation and associated clinical information of TCGA GBM were extracted from GDC Data Portal (https://portal.gdc.cancer.gov/). The RNA-seq transcriptome data and clinical traits of the CGGA GBM were downloaded from CGGA database (http://www.cgga.org.cn/). The microarray information of GSC expression was available in the Gene Expression Omnibus (GEO) database (GSE68029 at www.ncbi.nlm.nih.gov/geo).

Bioinformatics Analysis

Differential expression analysis

The limma R package was leveraged to identify differentially expressed genes (DEGs) between TMZ resistance and sensitive cell lines. The top 30 upregulated genes sorted according to p-value in TMZ resistant group were visualized using the pheatmap R package.

Single sample gene set enrichment analysis (ssGSEA)

To determine the abundance of GBM immune infiltration levels, immune gene signatures were obtained from data of Bindea et al. [30] to perform ssGSEA. The immune cell infiltration levels were estimated using “GSVA” R package based on deconvolution algorithm.

Gene set enrichment analysis (GSEA)

The gene sets of “c2.cp.kegg.v7.4”, “c5.go.bp.v7.4”, “verhaak glioblastoma mesenchymal” and “verhaak glioblastoma proneural” were obtained from The Molecular Signatures Database (MSigDB; http://www.gsea-msigdb.org/gsea/login.jsp) database for running GSVA. P-value < 0.05 indicates statistical significance.

Cell lines and cell culture

Human glioma cell lines U118MG, U87MG, LN229 and U251MG were purchased from the Chinese Academy of Sciences Cell Bank and cultured in DMEM medium (Gibco, USA) with 10% fetal bovine serum (FBS). The neural progenitor cell (NPC) and GBM patient-derived GSC cell lines and were kindly donated by Dr. Krishna P.L. Bhat (The University of Texas, M.D. Anderson Cancer Center, Houston, TX). GSC lines (GSC20, GSC267, GSC8–11) have been used extensively in previous studies and the subtypes of GSCs have been clarified according to the Verhaak or Philips gene signatures, respectively. GSCs and NPC were cultured in DMEM/F12 (Gibco, USA) with 2% B-27 no serum supplement (Gibco, USA), 20 ng/mL human recombinant bFGF (R&D Systems) as well as 20 ng/mL human recombinant EGF (R&D Systems, USA). The GSC or NPC spheres were digested using accutase solution (Sigma-Aldrich, USA). All cell lines were cultured in a humid chamber at 37°C and containing 5% carbon dioxide and 5% oxygen.

RNA extraction and quantitative real-time PCR (RT-qPCR)

TRIzol (Invitrogen, USA) was used to extract total RNA according to manufacturer's instruction. The high capacity cDNA Reverse Transcription Kit (Toyobo, China) was leveraged for reverse transcription in accordance with the manufacturer's protocol. An Mx-3000P Quantitative PCR System (Applied Biosystems, USA) was used for qRT-PCR.

Plasmids, Viral Transfections and Cloning

Human full-length PDIA3P1 as well as sh-PDIA3P1 plasmids were used in the current study for stable overexpression and knockdown, respectively, whereas empty plasmid was used as a control. Lentiviral particles were constructed by transfecting 293T cells with the packaging vectors psPAX2 and pMD2G. Lentiviral particles were collected 24 and 48 hours after transfection of 293T cells, filtered through a 0.45 μm filter (Corning), and then used to treat cells in culture. After 48 hours, cells were selected by Puromycin (2 μg/mL). All small interfering RNAs (siRNA) and overexpression plasmids were purchased from Genepharma (shanghai, China). For short-term knockdown and overexpression of GBM cells, cells were transfected of siRNAs and plasmids using the Lipofectamine 3000 kit (Invitrogen, USA) according to the manufacturer's instruction.

Reagents and antibodies

Temozolomide (TMZ) and Neflamapimod (NEF, Synonyms: VX-745) were purchased from MedChemExpress (MCE, https://www.medchemexpress.cn/). TMZ and NEF were dissolved in dimethyl sulfoxide (DMSO) at concentrations of 100 mM and 10 mM, respectively. TMZ and NEF in solvent are stored at -20 °C and used up within one month. The primary antibodies used in this study are listed as follows: β-actin (Cell Signaling Technology, 8480), CD44 (Cell Signaling Technology, 3570), C/EBPβ (Abcam, ab32358), YKL-40 (Cell Signaling Technology, 47066), SOX2 (Cell Signaling Technology, 3579), γ-H2AX (Cell Signaling Technology, 7631), MDM2 (Abcam, ab259265), JUN (Cell Signaling Technology, 9165), p-JUN (Cell Signaling Technology, 3270), ubiquitin (Cell Signaling Technology, 3933).

CCK-8 assay and drug treatment

CCK-8 reagent (RiboBio, China) was used to assess GBM cells viability. We seeded GBM cells in 96-well plates at a density of $2x10^3$ cells per well in 100 μl of Gibco DMEM containing 10% FBS. The cells were incubated at 37 °C 12 h for cells adhesion and then treated with different concentrations of TMZ or NEF. After incubation for 48 h, 10μl of CCK-8 solution was added to each well for 1h before measurement. Absorbance (OD value) at 450 nm was measured using a microplate.

Alkaline comet assay

The alkaline comet assay was used to detect the damaged DNA with high sensitivity [31]. GBM cells in different groups were harvested in PBS at a $1\text{-}3*10^5$ cells/ml density. Cells were mixed with molten LM agarose at a ratio of 1:10 (V/V) and 50 μl of the mixture was immediately pipetted onto a CometSlide. Then cells were lysed in alkaline lysis solution at 4℃ for 12 h for lysis. After that, the slides were soaked with alkaline electrophoresis buffer for 20 minutes away from light and electrophoresis for 30 min at 25V. After precipitation and washing, the slides were stained with Green-DNA Dye and images were captured by fluorescence microscopy.

Immunofluorescence (IF) assay

GBM cells were fixed in 4% paraformaldehyde for 15 min and washed three times in PBS. Then cells were permeabilized in 0.3% Triton X-100 for 10 min and blocked with 5% Goat serum for 1 h. Then the cells were incubated with indicated primary antibodies overnight at 4°C. Cells were then incubated with fuorescent second antibody at room temperature for 1 h. DAPI was used to counterstain nuclei for 15 min. Images were captured using a LeicaSP8 confocal microscope.

EdU assay

EdU cell proliferation assay kit (RiboBio, China) was used to determine cell proliferation. Cells were incubated with 200 μl of 5-ethynyl-20-deoxyuridine at 37 °C for 2 h. After fixed and permeabilized, the cells were incubated with Apollo reagent for 30 min and the Hoechst were used to stain nuclei. The images were viewed and obtained using fluorescence microscope.

Flow cytometry

Both suspended and adherent GBM cells were obtained for apoptosis analysis after treating with TMZ or DMSO (solvent control of TMZ) for 48 h. Annexin VFITC and PI staining (BD Biosciences, USA) was leveraged for apoptosis analysis according to the instruction. The number of cells were counted by BD Accuri C6 flow cytometer.

Colony formation assay

We seeded about 2000 GBM cells in 6-well plates per well in 1.5 ml of Gibco DMEM containing 10% FBS. The cells were incubated in a humidified chamber containing 5% CO2 and 5% O2 at 37 °C for 2 weeks. After that, colonies were fixed and stained with crystal violet (Solarbio, China) for 20 min. The colonies were washed with PBS for at least three times and the number of colonies were counted.

Neurosphere formation assay

We seeded about 1000 GSCs per well in 6-well plates with 1.5 ml DMEM/F12 containing 2% B-27. After 7 days incubation at 37 °C, the images were acquired and the relative diameters of neurospheres were calculated.

Extreme limiting dilution assay (ELDA)

We implanted GSCs into ultralow-attachment 96-well plates at densities of 0, 2, 4, 8, 16, 32, 64 and 128 cells per well in 10 replicates. The number of wells with neurospheres formation was counted after 7 days incubation. Collected data was analyzed using (http://bioinf.wehi.edu.au/software/elda/).

Protein half-life assay

CHX was used to inhibit new proteins synthesis. Cells were treated with 100 μg/ml CHX for 0 h, 2 h, 4 h, 6 h and 8 h prior to protein collection. The proteins levels were detected by western blot assay.

RNA pull-down assay and RNA immunoprecipitation (RIP) assay

Biotinylated PDIA3P1 and its anti-sense sequence were synthesized by RiboBio (GenePharma, China). Pierce™ Magnetic RNA-protein pull-down kit (Thermo Fisher Scientific, SA) was used for RNA pull-down assay. Cell lysates of GSC267 were firstly incubated with a biotin-labelled PDIA3P1 probe. Then the conjugated magnetic beads were added to cell lysates and the interacting proteins were separated by western blot and then the silver staining was used for visualization.

Magna RIP kit (Millipore, USA) was leveraged for RIP assay according to manufacturer's instruction. RT-qPCR was used for detecting the relative expression of immunoprecipitated RNA. The IgG antibody (from Magna RIP kit) was used for negative control.

Immunoprecipitation (IP) assay

The IP assay was performed using Pierce Classic Magnetic immunoprecipitation (IP)/Co-IP Kit (Thermo Fisher, USA) according to the manufacturer's instruction. Firstly, the different antibodies were incubated with protein A/G magnetic beads. Then the cell lysates from GSCs were collected and incubated with antibody coupled beads. The beads interacting proteins were washed and denatured and the proteins were examined using western blotting.

Drug combination analysis

To assess the combination of effect of TMZ and NEF, GBM cells were treated with different concentrations of TMZ and NEF for 48h in 3 replicates. CompuSyn software (Biosoft, Ferguson, MO, USA) was leveraged to evaluate drug synergism. The combination index (CI) values were calculated using non-constant ratios drug combination analysis according to instruction of the software. CI <0.75, CI=0.75–1.25, and CI >1.25 were defined as synergistic, additive, and antagonistic effects, respectively.

Animal studies

Luciferase labeled and stably transfected sh-PDIA3P1-U118MG cells or sh-Control-U118MG, or ov-PDIA3P1-U251 or ov-vector-U251 were injected into the brains of randomly grouped 4-week male BALB/c nude mice (5×10^5 cells/mouse). On the fifth postoperative day, the mice were randomly divided into TMZ treatment or control groups. Mice were treated with or without TMZ by oral gavage per week (5 mg/kg, p.o., 5 times per week). For evaluating the anti-tumor effect of TMZ in combination with NEF in vivo, luciferase-labeled GSC267 cells (1×10^6 cells/mouse) were implanted into the brains of 4-week male BALB/c nude mice. After 7 days post-operative, the mice were randomly divided into four groups, control, TMZ only (5 mg/kg, p.o.,5 times per week), NEF only (5 mg/kg, p.o.,5 times per week) and combination group. To evaluate the intracranial tumor, bioluminescence imaging was used to quantify tumor burden using an IVIS Lumina Series III (PerkinElmer). All procedures used for animal treatments and experiments were approved by and under the requirements of the Animal Care and Use Committee of the Qilu Hospital of Shandong University.

Statistical analysis

All statistical analysis was conducted by R 4.0.1 and GraphPad Prism 8.0 software. Two-group comparisons were conducted with Student's t-Test and represented as mean ± SD unless noted otherwise. For comparisons among more than two groups, the one-way ANOVA and the Wilcoxon test were used for parametric data and non-parametric respectively. P-value < 0.05 was considered statistically significant (*p-value < 0.05; **p-value < 0.01; ***p-value < 0.001). The receiver operating characteristic (ROC) curve was used to evaluate the diagnostic value of PDIA3P1, and the area under the curve (AUC) was quantified using the pROC R package. Pearson correlation was used to calculate the correlation between two or more groups. Kaplan-Meier curve and log-rank test were used to evaluate survival between different groups.

Results

PDIA3P1 is markedly upregulated in TMZ-resistant cell lines and promotes TMZ resistance.

To search for potential lncRNAs involved in GBM resistance to TMZ chemotherapy, the information of 10 glioma cell lines paired with specific half-maximal inhibitory concentration (IC50) values of TMZ were obtained from GDSC and the RNA-seq data of corresponding cell lines was downloaded from the CCLE. We divided the glioma cell lines into TMZ resistance group and TMZ sensitive group based on IC50 values. The limma package was utilized to analyze the DEGs between the two groups. The clustered

heatmap (Fig. 1A) exhibited the top 30 upregulated genes in TMZ resistant group sorted according to p-value. Among the DEGs, PDIA3P1 is markedly upregulated in TMZ resistance cell lines (log_2Fold change = 1.6, $P < 0.001$) (Fig. S1A and Table. S1). Based bioinformatic analysis, we found that the expression of PDIA3P1 was significantly upregulated in most recurrent gliomas (Fig. 1B). Survival analysis exhibited that higher PDIA3P1 levels were related to poorer progression-free survival (PFS) in GBM patients (Fig. S1B). In addition, the low-PDIA3P1 group showed a significant survival advantage in GBM patients either receiving or not receiving chemotherapy (Fig. 1C). Next, qRT-PCR on two TMZ-sensitive (U251 and LN229) and TMZ-resistant GBM cell lines (U118MG and U87MG) verified that PDIA3P1 was upregulated in TMZ-resistant cell lines (Fig. S1C).

To investigate the functional role of PDIA3P1 in promoting TMZ resistance, PDIA3P1 was knocked down using two independent shRNAs in U118MG and U87MG and overexpressed in U251 and LN229. The expression of PDIA3P1 was detected using qRT-PCR (Fig. S1D). Knockdown of PDIA3P1 in resistant cell lines (U118MG and U87MG) resulted in a notably reduction in IC_{50} and further inhibition of tumor cell growth rate upon TMZ treatment (Fig. 1D and Fig. S1E). In contrast, overexpression of PDIA3P1 in sensitive cell lines (U251 and LN229) resulted in a significant increase of IC_{50} values and counteracted inhibitory effect of TMZ on tumor cells growth (Fig. 1E and Fig. S1E).

To evaluate the effect of PDIA3P1 on the TMZ-resistant phenotype in vivo, 5×10^5 luciferase-labeled U118MG-shPDIA3P1 or U118-shNC, and U251-PDIA3P1 or U251-Vector cells were injected into nude mice, respectively. We tracked tumor proliferation through in vivo bioluminescence imaging. Despite the initial tumor size being similar (Fig. S2A and Fig. S2B), xenografts bearing U118MG-shPDIA3P1 cells showed significant tumor growth inhibition, whereas xenografts bearing U251-PDIA3P1 cells showed tumor growth promotion. As expected, TMZ treatment (5 mg/kg, p.o., 5 times per week) reduced tumor burden. Tumor size in U118MG-shPDIA3P1 group was reduced compared to control group (Fig. 1F and Fig. 1G), while tumor size in U251-PDIA3P1 group was relatively increased compared to control group (Fig. 1H and Fig. 1I). Consistently, Kaplan-Meier curves revealed that the overall survival time of mice in PDIA3P1 knockdown group was prolonged with and without TMZ treatment (Fig. S2C). Although TMZ treatment significantly prolonged the survival time of mice in U251-Vector group, PDIA3P1 overexpression shortened the survival time of mice in both the treatment and control groups (Fig. S2D). H&E-stained mice brain sections showed that knockdown of PDIA3P1 greatly reduced tumor invasiveness, with or without TMZ treatment, whereas overexpression of PDIA3P1 promoted tumor invasiveness (Fig. S2E and Fig. S2F). Taken together, these findings indicated that PDIA3P1 promoted glioma cells resistance to TMZ both in vitro and in vivo.

Knockdown of PDIA3P1 exacerbates DNA damage and proliferation inhibition induced by TMZ intervention.

To explore the biological behaviors of PDIA3P1, we performed GSVA enrichment. PDIA3P1 high expression group was significantly enriched in damage repair and stress response pathways such as the regulation of DNA repair and cellular response to chemical stress, suggesting that PDIA3P1 may play a

role in damage repair and stress response (Fig. S3A and Table. S2). As TMZ exerts its antitumor effects mainly by damaging DNA and inducing programmed cell death (PCD), we performed COMET and γH2AX assays to detect DNA damage. Alkaline COMET assay could be used for sensitive detection of DNA double-strand breaks (DSBs) and single-strand breaks. We found increased DNA damage in shPDIA3P1 cells after TMZ treatment, whereas knockdown of PDIA3P1 had very little effect on DNA damage in the absence of TMZ in U118MG and U87MG cells (Fig. 2A, Fig. S4A and Fig. 2B). Phosphorylated histone H2AX (γH2AX) is an indicator of the DNA damage response (DDR). When DNA damage occurs, γH2AX can be recruited to the lesions[32]. Using IF staining assay, we confirmed that knockdown of PDIA3P1 increased nuclear γH2AX levels after TMZ treatment, while nuclear γH2AX levels remained virtually unchanged in the absence of TMZ intervention. (Fig. 2C, Fig. S4B and Fig. 2D). We further performed EdU, colony formation and apoptosis assays to explore the function of PDIA3P1. EdU and colony formation assays showed that knockdown of PDIA3P1 inhibited cell proliferation, whereas in the case of TMZ treatment, knockdown of PDIA3P1 inhibited cell growth even more (Fig. 2E, Fig. S4C and Fig. S4D). Then we recorded apoptosis rate using flow cytometry and the proportion of apoptotic cells significantly increased in PDIA3P1 knockdown group after TMZ treatment (Fig. 2F). Collectively, the above results indicated that knockdown of PDIA3P1 exacerbated TMZ intervention induced DNA damage and growth inhibition, thereby restoring the sensitivity of tumor cells to TMZ.

Overexpression of PDIA3P1 counteracted TMZ treatment-induced DNA damage and growth inhibition.

Since knockdown of PDIA3P1 was able to restore the TMZ sensitivity of GBM cells, we investigated whether overexpression of PDIA3P1 could promote TMZ resistance. We overexpressed PDIA3P1 in U251 and LN229 GBM cell lines which are relatively sensitive to TMZ. Comet assay showed that PDIA3P1 overexpression without TMZ intervention had little effect on the DNA damage, while overexpression of PDIA3P1 could salvage TMZ-induced DNA damage (Fig. 3A and Fig. S4E). Similarly, IF staining assay found that PDIA3P1 overexpression decreased nuclear γH2AX levels after TMZ treatment, whereas nuclear γH2AX levels remained almost constant and at a relatively low level in the absence of TMZ (Fig. 3B and Fig. S4F). The EdU assay exhibited that overexpression of PDIA3P1 had a positive effect on cell proliferation. Furthermore, PDIA3P1 overexpression partially counteracted TMZ-mediated cell growth inhibition (Fig. 3C). We then evaluated the effect of PDIA3P1 overexpression on the apoptosis rate of GBM cells. As shown in Fig. 3D, a slight decrease in apoptosis rate was observed in these cells overexpressing PDIA3P1 compared to control cells without TMZ treatment, whereas PDIA3P1 overexpression greatly counteracted the apoptosis induced by TMZ treatment (Fig. 3D). Hence, through a series of experiments, we demonstrated that overexpression of PDIA3P1 could reduce DNA damage and proliferation inhibition caused by TMZ intervention, thus conferring TMZ resistance to GBM cells.

Elevated expression of PDIA3P1 is associated with Mesenchymal subtype.

We have used gain-of-function and loss-of-function experiments in vitro and in vivo to prove that PDIA3P1 can promote GBM cells resistance to TMZ by reducing DNA damage. We intend to further investigate the mechanism of PDIA3P1-mediated TMZ resistance. Phenotypic heterogeneity and

plasticity in GBM drive therapy resistance and recurrence. Compared to PN subtype, which has a better survival prognosis and is sensitive to TMZ treatment, the MES subtype shows a higher resistance to radiotherapy and chemotherapy and a higher risk of recurrence. [25, 33]. We hypothesized that the function of PDIA3P1 to promote TMZ resistance is mediated by affecting GBM subtypes. We first examined the expression of PDIA3P1 in TCGA and CGGA datasets and found that PDIA3P1 expression was significantly higher in the MES subtype than in the PN subtype (Fig. 4A and Fig. S5A). The existence of GSCs is an important factor contributing to GBM heterogeneity and TMZ resistance, and GSCs are used as a valuable experimental model for GBM analysis. By detecting PDIA3P1 expression by qRT-PCR, we concluded that PDIA3P1 expression was markedly upregulated in MES GSCs (GSC20, GSC267) compared with PN GSCs (GSC8-11, GSC11), and PDIA3P1 was least expressed in neuronal precursor cell lines (NPC) (Fig. 4B). To explore the predictive efficiency of PDIA3P1 for GBM subtype, the area under the receiver operating characteristic (ROC) curve (AUC) was calculated and PDIA3P1 expression was found to be accurate in assessing GBM subtypes (AUC = 0.7687) (Fig. 4C and Fig. S5B). Meanwhile, we performed pearson correlation analysis of gene expression and found a significant positive correlation between PDIA3P1 and MES subtype-related genes (CD44, FN1, CHI3L1, SERPINE1), while PDIA3P1 was negatively correlated with PN subtype-related genes (DLL3, NCAM1, ASCL1, OLIG2) (Fig. 4D). We further performed a GSEA analysis of the relationship between PDIA3P1 and GBM subtypes based on the TCGA dataset. As the results showed, the MES-GBM subtype was enriched at high PDIA3P1 expression group, whereas the PN-GBM subtype presented in the low PDIA3P1 expression group (Fig. 4E). The two independent shRNAs were transfected into GSC20 and GSC267, and PDIA3P1 was overexpressed in GSC8-11 to investigate the causal relationship between PDIA3P1 and GBM subtype (Fig. S5C). Stable knockdown of PDIA3P1 in GSC20 and GSC267 resulted in an obvious inhibition of tumorsphere expansion (Fig. S5D) and reduced sphere formation ability (Fig. 4G). The above results demonstrated that PDIA3P1 was associated the ability of tumorigenesis and stemness of GSCs. CD44 and SOX2 are marker proteins of the MES and PN subtypes, respectively. In GSC20 and GSC267, PDIA3P1 knockdown decreased CD44 expression and increased SOX2 expression, which was verified by IF assays (Fig. 4D and Fig. S5E). Besides, two MES marker proteins CD44 and YKL-40 were downregulated after interfering with PDIA3P1 expression (Fig. 4H).

PDIA3P1 promotes PMT and TMZ resistance by affecting C/EBPβ in GSCs.

Given that LncRNAs can directly bind to proteins to exert regulatory functions, we first performed RNA pull-down experiments in GSC267 to explore the molecular interaction mechanism of PDIA3P1. Then we detected the binding proteins of PDIA3P1 by silver staining and mass spectrometry analysis (Table. S4). We found that C/EBPβ was significantly enriched on PDIA3P1 compared to antisense, and RNA pull down assay was performed again to verify their interaction (Fig. 5A and Fig. 5B). Subsequently, RNA immunoprecipitation (RIP) assay further confirmed that C/EBPβ could specifically combine with PDIA3P1 (Fig. 5C). C/EBPβ is thought to be one of the MRs promoting PMT, and the interaction and effect of PDIA3P1 on C/EBPβ expression further validated our finding that PDIA3P1 can be involved in GBM PMT progression. Knockdown of PDIA3P1 decreased the expression of C/EBPβ, CD44 and YKL-40, whereas transfection of C/EBPβ into GSC267 counteracted the effect of PDIA3P1 knockdown on the expression of

CD44 and YKL-40 (Fig. 5D). We further performed neurosphere formation and extreme limiting dilution assay (ELDA) to explore the effect of PDIA3P1- C/EBPβ on tumorigenesis. We observed the expansion of tumor spheres and the ability to form spheres were significantly restored when C/EBPβ was transfected into PDIA3P1-knckdown GSC267 cells (Fig. 5E and Fig. 5F). Knockdown of C/EBPβ in PDIA3P1-expressing GSC8-11 resulted in the suppression of tumorsphere expansion (Fig. 5G) and reduced sphere formation ability (Fig. 5H). To investigate that PDIA3P1 promotes the resistance of GSCs to TMZ by affecting C/EBPβ, the comet assay and γ-H2AX IF assay were performed. The results showed that knockdown of PDIA3P1 increased nuclear γ-H2AX levels in GSC267 after TMZ treatment, whereas transfection of C/EBPβ into shPDIA3P1-GSC267 decreased nuclear γ-H2AX expression, implying that overexpression of C/EBPβ restores TMZ resistance of GSCs (Fig. 5I and Fig. S6A). Similar results were obtained for the comet experiment (Fig. 5I and Fig. S5B), which suggests that overexpressing C/EBPβ could counteract the effect of PDIA3P1 knockdown on TMZ resistance in GSCs. For GSC8-11, comet assay and γ-H2AX IF assay revealed that knockdown of C/EBPβ restored the sensitivity of GSC8-11 expressing PDIA3P1 to TMZ (Fig. 5J, Fig. S6C and Fig. S6D). Collectively, we determined that PDIA3P1 promoted PMT and TMZ resistance by affecting C/EBPβ expression.

PDIA3P1 stabilizes C/EBPβ by preventing MDM2 -mediated ubiquitination.

We further investigate the interaction of PDIA3P1-C/EBPβ. PDIA3P1 knockdown decreased protein expression of C/EBPβ (Fig. 5D and Fig. 5K), but not mRNA levels of C/EBPβ (Fig. S6E), suggesting that PDIA3P1 regulates protein level of C/EBPβ through affecting translational or post-translational modification. The ubiquitin-proteasome system (UPS) is the main pathway of protein degradation, and it participates in the degradation of more than 80% of proteins in cells [34]. To confirm the possibility of that PDIA3P1 regulates C/EBPβ through proteasome, the GSCs were treated with the proteasome inhibitor MG132. Knockdown of PDIA3P1 significantly decreased the expression of C/EBPβ, whereas, MG132 treated GSCs with silenced PDIA3P1 showed minimal change in C/EBPβ levels (Fig. 5K). Then we blocked the protein synthesis using cycloheximide (CHX) and found that PDIA3P1 knockdown resulted in a significantly shorter half-life of C/EBPβ protein in GSC267 (Fig. 5L). Consistently, the half-life of C/EBPβ protein in PDIA3P1 stable overexpression GSC8-11 was significantly longer than that of the corresponding control cells (Fig. S6F). Immunoprecipitation (IP) results showed that knockdown of PDIA3P1 significantly increased the ubiquitylation of C/EBPβ in GSC267, whereas overexpression of PDIA3P1 significantly decreased the ubiquitylation of C/EBPβ in GSC8-11 (Fig. 5M). Above all, our data suggested that PDIA3P1 was involved in the post-translational modification of C/EBPβ.

E3 ubiquitin ligase is a family of more than 700 proteins, binding ubiquitin to the target protein and play a major role in protein degradation[34]. To further investigate the E3 ubiquitin ligases involved in the post-translational modification of C/EBPβ, we reviewed numerous references and found that Mouse double minute 2 homolog (Mdm2) could target C/EBPβ for degradation [35]. MDM2 is an E3 ubiquitin ligase of the RING finger family that is known to be involved in the degradation of p53 [36]. Since we have proved that PDIA3P1 directly binds to C/EBPβ to affect the ubiquitination level of C/EBPβ, we supposed that PDIA3P1 may impact on the C/EBPβ-MDM2 complex formation. To test our hypothesis, the interaction

between C/EBPβ and MDM2 was investigated by co-IP assays. The results demonstrated that overexpression of PDIA3P1 hampered the interaction of C/EBPβ and MDM2 in GSC267 (Fig. 5N). In addition, knockdown of PDIA3P1 resulted in more MDM2 binding to C/EBPβ in GSC267 (Fig. 5N). Collectively, our present data suggested that PDIA3P1 could stabilize C/EBPβ by disrupting C/EBPβ-MDM2 complex.

Pdia3p1 Is Upregulated In Response To Tmz-induced Activation Of The P38-mapk Signaling Pathway

TMZ treatment and subsequent detrimental stress within tumor cells can change expression levels of multiple genes. We treated GSC20, GSC267, U118MG and U251 using different concentrations of TMZ for 48 h, as well as cells with 400 μM TMZ for different treatment durations. We observed that PDIA3P1 expression was upregulated in a dose-dependent and time-dependent manner following TMZ intervention (Fig. 6A and Fig. 6B). To explore the mechanism of TMZ-induced PDIA3P1 upregulation, we obtained RNA array data from GSE68029, which identified defense profiles of GSC-500uM TMZ. We performed differential analysis of this data and conducted gene oncology (GO) enrichment analysis on the differential genes. Compared with parental GSCs, TMZ treatment resistant GSCs were significantly enriched in the gene sets associated with p38α MAPK biological pathway, which suggested that the p38α MAPK signaling pathway was possibly involved in TMZ resistance and was activated after TMZ treatment of GSCs (Fig. 6C). The p38α MAPK signaling pathway is mainly responsible for transduction of extracellular signals, which can be activated by various environmental stresses and inflammatory cytokines [37]. Activation of the core molecule p38α indirectly regulates the transcriptional process of various genes by regulating multiple transcription factors, which helps cells to respond adequately to changing environmental conditions [38].

Targeting p38α may block the stress response of tumor cells, thus preventing TMZ-induced upregulation of PDIA3P1. We reviewed small molecule inhibitors specifically targeting p38 from DRUGBANK and MCE. We screened Neflamapimod (NEF) is a potential drug for the treatment of Alzheimer's disease (AD) and has been preliminarily confirmed to be safe for human use [39]. NEF has excellent blood-brain barrier (BBB) permeability, which suggests its value for central nervous system (CNS) disorders and some studies have exhibited the anti-tumor activity of NEF [40–42]. CCK-8 cell proliferation was performed to determine IC_{50} of four cell lines for NEF (Fig. 6D). GBM cells treated with NEF could inhibited TMZ-induced upregulation of PDIA3P1 (Fig. 6E). Then, we further explored whether TMZ in combination with NEF could synergistically inhibit GBM cells growth. GBM cells were treated with indicated concentrations of TMZ and NEF, respectively and the cell growth inhibition was determined by CCK-8 assay (Fig. 6F). Based the results of proliferation inhibition, we calculated combination index (CI) score to evaluate the combination effect of TMZ and NEF (Fig. 6G and Fig. S7A). $CI > 1.25$, $CI = 0.75–1.25$, and $CI < 0.75$ were defined as antagonistic, additive and synergistic effects, respectively. For instance, in GSC267 cells, a relative low concentration of TMZ (50 μM) and NEF (20 μM) may exhibit better synergistic effect (CI = 0.44), despite their relatively low growth inhibitory effects about 23%. When GSC20 cells were treated with moderate concentrations of TMZ (800 μM) and NEF (80 μM), they showed an additive effect despite their

relatively high growth inhibition of about 81%. Collectively, these data revealed that TMZ in combination with NEF exhibited synergistical effects at the indicated concentrations.

Activation of p38-MAPK signaling pathway could further activate some transcriptional factors like JUN. We observed a significantly positive relationship between the expression of JUN and PDIA3P1 in TCGA and CGGA datasets (Fig. 6H). Knockdown of JUN not only reduced the PDIA3P1 expression, but also counteracted TMZ-induced upregulation of PDIA3P1 (Fig. 6I), preliminarily suggesting that JUN is responsible for PDIA3P1 transcription. We constructed four fragments of different lengths located upstream of the TSS based on the JUN binding motif (Fig. 6J). The four luciferase reporter plasmids were transfected into GSC267 individually to verify the JUN binding sites. The luciferase activity of fragment 4 was statistically unchanged after knockdown of JUN, demonstrating that JUN does not bind to fragment 4 (Fig. 6K). To further determine the binding sites in more detail, we designed three pairs of PCR primers and performed CHIP assay. qRT-PCR assay showed approximate 10-fold enrichment and 5-fold enrichment for site #1 and site #2, respectively, while there was no significant enrichment at site #3 (Fig. 6L and Fig. S7B). In conclusion, our data suggest that JUN is involved in TMZ-induced upregulation of PDIA3P1 and can directly bind and initiate PDIA3P1 transcription.

NEF combined with TMZ confers a better anti-tumor effect both in vitro and in vivo.

To evaluate the antitumor effect of TMZ and NEF combination, we conducted a series of experiments in vitro. In GSC20 and GSC267 cells, the comet assay showed that the level of DNA damage was higher when treated with TMZ or NEF alone than in the control group, while DNA damage was more pronounced in the combination treatment group than in the monotherapy, indicating that the combination of TMZ and NEF exhibited a more powerful anti-tumor effect (Fig. 7A and Fig. 7B). Similar results were obtained in the γH2AX IF assay, where significantly higher nuclear γH2AX was observed in the combined group of TMZ and NEF, suggesting that the combined treatment resulted in a potentially enhanced effect of DNA damage (Fig. 7C and Fig. 7D). The EdU assay showed that both TMZ or NEF treatment alone could inhibit proliferation of tumor cells, whereas the combination group had a more obvious inhibition of proliferation efficiency (Fig. S8A). Next, we detected apoptosis levels using flow cytometry. U118MG with TMZ or NEF treatment alone exhibited 31.35% and 30.22% apoptosis rates, respectively, whereas the apoptosis rate increased to 51.2%, when TMZ combined with NEF was employed (Fig. S8B). Given that NEF targeted p38α and thereby affected the subsequent transcriptional process of PDIA3P1, which have been shown to promote PMT, we intend to verify whether NEF is also involved in the subtype of GSC. As the results showed, the expression of CD44 was significantly reduced in GSC20 and GSC267 after 48 hours of NEF (50 μM) treatment, while the expression of SOX2 was elevated (Fig. 7E and Fig. 7F). In addition, overexpression of PDIA3P1 counteracted the effect of NEF treatment on CD44 and SOX2 expression, indicating that NEF could affect the subtypes of GSC through PDIA3P1 (Fig. 7E and Fig. 7F). To evaluate the antitumor activities of TMZ and/or NEF in vivo, nude mice carrying GSC267 xenografted tumors were administered TMZ (5mg/kg, p.o., 5 days per week), NEF (5 mg/kg/day, p.o., 5 days per week), or both drugs in combination after building the orthotopic xenograft model. The results showed that both TMZ or NEF treatment alone could inhibit proliferation of tumor cells, whereas the combination treatment

produced remarkable tumor regression (Fig. 7G and Fig. S8C). Consistently, survival analysis showed that both TMZ or NEF treatment alone could prolong the survival time of mice, whereas the combination treatment group showed a significantly longer survival time (Fig. S8D). H&E-stained mouse brain sections showed that TMZ in combination with NEF limited the invasion ability of the tumor to the greatest extent (Fig. S8E). Taken together, our results exhibited that TMZ in combination with NEF had an excellent synergistic anti-tumor effect both in vitro and in vivo.

Discussion

In this study, we screened the LncRNA PDIA3P1, which was closely related to TMZ resistance in GBM, based on the comprehensive analysis of CCLE and GDSC database. Bioinformatic analyses of public databases combing qRT-PCR results indicated that the expression of PDIA3P1 was upregulated in TMZ resistance cell lines and predicted higher risk of tumor recurrence. Combining in vitro and in vivo assays, we further confirmed that PDIA3P1 could reduce the TMZ sensitivity of glioma cell lines. Mechanistically, PDIA3P1 promoted PMT by disrupting the C/EBPβ/MDM2 complex to inhibit the ubiquitination of C/EBPβ, thereby enabling glioma cells to obtain stronger TMZ therapy resistance. To our knowledge, this is the first report showing the function and mechanism of PDIA3P1 promoting TMZ resistance in GBM.

The main obstacle to GBM therapy is the development of TMZ resistance. Increasing evidence suggests that excessive activation of O6-methylguanine-DNA methyltransferase (MGMT), which removes TMZ-induced alkylation from different nucleotides, is the most important cause of TMZ resistance in GBM[43–45]. However, studies have shown that MGMT overexpression is not the only determinant contributing to GBM resistance to TMZ recently [5]. Some other factors such as the advent of GSCs, over-activation of DNA repair pathways, favorable autophagy, decreased drugs influx and increased drugs efflux, facilitate drug resistance in TMZ other than MGMT overexpression[46–51]. GSCs exhibit the capacity of self-renewal, immortal propagation as well as multilineage differentiation[52]. GSC can be divided into PN and MES subtypes according to transcription program, genotype and epigenetic status[53–55]. PN-GSC is characterized by relatively faster proliferation and sensitive to adverse stimulation, whereas MES-GSC is characterized by the secretion of various factors and the ability to maintain relative stability under adverse conditions[33]. PN subtype transition to MES subtype is considered to be a crucial process for tumor recurrence and treatment tolerance in GBM[56]. It was reported that the immune infiltration in tumor microenvironment (TME) was associated with PMT. However, our analysis indicated that the expression of PDIA3P1 was not associated with tumor immunity (Fig. S3B and Table. S3), suggesting the impact of PDIA3P1 on PMT based a endogenous pathway.

C/EBPβ is highly expressed and activated in MES subtype GSC and it is the master regulator in the process of PMT. Given its role in the PMT, C/EBPβ has great potential as a therapeutic target for GBM[26]. However, the mechanisms for C/EBPβ regulation in GBM are not completely clarified. Based on RNA pull down and mass spectrometry analysis, we concluded PDIA3P1 promoted PMT by targeting C/EBPβ. We found that PDIA3P1 had no effect on mRNA expression, but increased C/EBPβ protein expression in GSCs by increasing C/EBPβ protein stability and decreasing C/EBPβ ubiquitination. Therefore, our results

suggested that PDIA3P1 could function as a PMT regulator through restricting C/EBPβ degradation. PDIA3P1 have been propounded to primarily function as a competitive endogenous RNA (ceRNA) that compete for microRNA (miRNA) binding, thereby playing an important role in gene regulation[57–59]. In this study, PDIA3P1 did not function as a ceRNA but was able to physically bind to C/EBPβ protein, thereby reducing its ubiquitination and subsequent degradation. The ubiquitin-dependent protein degradation plays critical role in post-transcriptional regulation of most proteins[60]. It has been reported that C/EBPβ could be degraded by E3 ubiquitin ligase MDM2 to promote myogenesis[61]. Therefore, we hypothesized and verified that PDIA3P1 has an effect on the ubiquitination degradation of C/EBPβ by MDM2. Our data suggest that PDIA3P1 can bind proteins that function to disrupt the C/EBPβ/MDM2 complex rather than binding to miRNAs.

The function of p38α-MAPK pathway is to relay, amplify and integrate a variety of extracellular stress such as radiotherapy, chemotherapy, hypoxia and hunger, thereby regulating the genomic and physiological response of cells to their environment[62]. It has been reported that acute treatment with TMZ could induce DNA damage and a transitory activation of MAPK14/ p38α[63, 64]. Besides, activation of MAPK pathway was associated with poor survival among GBM patients during the TMZ era[65]. It is obvious that p38α-MAPK pathway is activated during TMZ treatment and resist the killing effect of TMZ. We found that the expression of PDIA3P1 increased after treatment of cells with TMZ in a concentration gradient and time-gradient-dependent manner. Further analyses indicated that it was the p38α-MAPK signaling pathway that mediated TMZ-induced upregulation of PDIA3P1. There was a loop that TMZ treatment activated p38α-MAPK signaling pathway, which then promoted the expression of PDIA3P1, and finally PDIA3P1 could promote PMT to reduce the adverse effects of TMZ treatment. We aim to set up interventions to break this loop and provide potential therapy strategies for overcoming TMZ resistance.

Currently, TMZ combined with other antitumor agents has become the main strategy for the treatment of refractory gliomas [66]. The basic principle of combination treatment is to leverage different agents that target key pathways by different mechanisms to reduce drug-resistant cancer cells. There was evidence that combination therapy with TMZ prolonged the overall survival time of GBM patients[67]. Based on the strategy of combination therapeutics, we have selected a selective p38α inhibitor, NEF, which has blood-brain barrier permeability. We revealed that NEF in combination with TMZ could exhibit synergistic effects at indicated concentrations. Moreover, we proved the effectiveness of the combined treatment strategy through in vitro and in vivo experiments. In summary, we identified the mechanism of PDIA3P1 mediating TMZ resistance. More importantly, we offered a new treatment strategy in which the combined use of TMZ and NEF had the potential to overcome TMZ resistance.

Conclusions

In conclusion, PDIA3P1 promoted PMT through stabilization of C/EBPβ, thereby conferring GBM cells TMZ resistance. P38α-JUN was responsible for transcriptional upregulation of PDIA3P1 induced by TMZ intervention. P38α targeted drug NEF could prevent the TMZ induced upregulation of PDIA3P1. NEF

combined with TMZ exhibited an excellent synergistic anti-tumor effect (Fig. 8H). Our research provided clinical translational basis for the possibility of overcoming TMZ resistance and recurrence of GBM.

Abbreviations

GBM: Glioblastoma

TMZ: Temozolomide

BBB: Blood-brain barrier

PDIA3P1: Protein disulfide isomerase family A, member 3 pseudogene 1

C/EBPβ: CCAAT/enhancer binding protein (C/EBP), beta

TME: Tumor microenvironment

TCGA: The Cancer Genome Atlas

CGGA: Chinese Glioma Genome Atlas

IF: Immunofluorescence

NEF: Neflamapimod

MGMT: O6-methylguanine-DNA methyltransferase.

Declarations

Ethics approval and consent to participate

The study was authorized by the Ethics Committee of Qilu Hospital. The human cancer tissues used in this study were approved by the Ethics Committee of Qilu Hospital (No. DWLL-2021-090).

Consent for publication

All authors give consent for the publication of the manuscript in Molecular Cancer.

Availability of supporting data

All the data obtained and/or analyzed during the current study were available from the corresponding authors on reasonable request.

Competing interests

The authors declare that they have no competing interests.

Funding

This work was supported by grants from the National Natural Science Foundation of China (Nos. 81874083; 82072776; 82072775; 81702468; 81802966; 81902540□81874082; 81472353), Natural Science Foundation of Shandong Province of China (Nos. ZR2019BH057□ZR2020QH174; ZR2021LSW025), the Jinan Science and Technology Bureau of Shandong Province (2021GXRC029), Key clinical Research project of Clinical Research Center of Shandong University (2020SDUCRCA011) and Taishan Pandeng Scholar Program of Shandong Province (No. tspd20210322).

Authors' contributions

GL and PZ supervised the project. ZJG designed the research and performed all experiment. JYX and YF completed the basic experiment part. YHQ and WSB performed statistical analysis. SLZ, XG, LD, and RRZ helped to revise the manuscript. CS and HX helped advise on this research design. All authors read and approved the final manuscript.

Corresponding author

Correspondence to Gang Li and Ping Zhang.

Acknowledgments

We thank Dr. Sun (Immune Regulation in Cancer, Germany Cancer Research Center) for his patient and constructive comments and guidance on this study. We are grateful to Dr. Frederick F. Lang and Dr. Krishna P.L. Bhat for providing GSC cell lines used in our study.

Author’s information

Affiliations

Department of Neurosurgery, Qilu Hospital, Cheeloo College of Medicine and Institute of Brain and Brain-Inspired Science, Shandong University, Jinan 250012, Shandong, China

Zijie Gao, Jianye Xu, Yang Fan, Yanhua Qi, Shaobo Wang, Shulin Zhao, Xing Guo, Hao Xue, Lin Deng, Rongrong Zhao, Ping Zhang & Gang Li

Immune Regulation in Cancer, Germany Cancer Research Center (DKFZ), Heidelberg, 69120, Germany

Chong Sun

References

1. Van Meir E, Hadjipanayis C, Norden A, Shu H, Wen P, Olson JJCacjfc: **Exciting new advances in neuro-oncology: the avenue to a cure for malignant glioma**. 2010, **60**(3):166–193.

2. Malzkorn B, Reifenberger GJCoio: **Practical implications of integrated glioma classification according to the World Health Organization classification of tumors of the central nervous system 2016**. 2016, **28**(6):494–501.
3. Villani V, Anghileri E, Prosperini L, Lombardi G, Rudà R, Gaviani P, Rizzato S, Lanzetta G, Fabi A, Scaringi C *et al*: **Adjuvant chemotherapy after severe myelotoxicity during chemoradiation phase in malignant gliomas. Is it feasibile? Results from AINO study (Italian Association for Neuro-Oncology)**. 2021, **268**(8):2866–2875.
4. Shergalis A, Bankhead A, Luesakul U, Muangsin N, Neamati NJPr: **Current Challenges and Opportunities in Treating Glioblastoma**. 2018, **70**(3):412–445.
5. Tomar M, Kumar A, Srivastava C, Shrivastava AJBebaRoc: **Elucidating the mechanisms of Temozolomide resistance in gliomas and the strategies to overcome the resistance**. 2021:188616.
6. Strobel H, Baisch T, Fitzel R, Schilberg K, Siegelin M, Karpel-Massler G, Debatin K, Westhoff MJB: **Temozolomide and Other Alkylating Agents in Glioblastoma Therapy**. 2019, **7**(3).
7. Moody C, Wheelhouse RJP: **The medicinal chemistry of imidazotetrazine prodrugs**. 2014, **7**(7):797–838.
8. Lee SY: **Temozolomide resistance in glioblastoma multiforme**. Genes Dis 2016, **3**(3):198–210.
9. Cech T, Steitz JJC: **The noncoding RNA revolution-trashing old rules to forge new ones**. 2014, **157**(1):77–94.
10. Kopp F, Mendell JJC: **Functional Classification and Experimental Dissection of Long Noncoding RNAs**. 2018, **172**(3):393–407.
11. Ulitsky I, Bartel DJC: **lincRNAs: genomics, evolution, and mechanisms**. 2013, **154**(1):26–46.
12. Palazzo A, Koonin EJC: **Functional Long Non-coding RNAs Evolve from Junk Transcripts**. 2020, **183**(5):1151–1161.
13. Voce DJ, Bernal GM, Wu L, Crawley CD, Zhang W, Mansour NM, Cahill KE, Szymura SJ, Uppal A, Raleigh DR *et al*: **Temozolomide Treatment Induces lncRNA MALAT1 in an NF-kappaB and p53 Codependent Manner in Glioblastoma**. Cancer Res 2019, **79**(10):2536–2548.
14. Lu C, Wei Y, Wang X, Zhang Z, Yin J, Li W, Chen L, Lyu X, Shi Z, Yan W *et al*: **DNA-methylation-mediated activating of lncRNA SNHG12 promotes temozolomide resistance in glioblastoma**. Mol Cancer 2020, **19**(1):28.
15. Zhang MX, Zhang LZ, Fu LM, Yao HH, Tan L, Feng ZH, Li JY, Lu J, Pan YH, Shu GN *et al*: **Positive feedback regulation of lncRNA PVT1 and HIF2alpha contributes to clear cell renal cell carcinoma tumorigenesis and metastasis**. *Oncogene* 2021.
16. Tang D, Luo Y, Jiang Y, Hu P, Peng H, Wu S, Zhang G, Wang Y: **LncRNA KCNQ1OT1 activated by c-Myc promotes cell proliferation via interacting with FUS to stabilize MAP3K1 in acute promyelocytic leukemia**. Cell Death Dis 2021, **12**(9):795.
17. Xiu B, Chi Y, Liu L, Chi W, Zhang Q, Chen J, Guo R, Si J, Li L, Xue J *et al*: **LINC02273 drives breast cancer metastasis by epigenetically increasing AGR2 transcription**. Mol Cancer 2019, **18**(1):187.

18. Chen R, Nishimura M, Bumbaca S, Kharbanda S, Forrest W, Kasman I, Greve J, Soriano R, Gilmour L, Rivers C *et al*: **A hierarchy of self-renewing tumor-initiating cell types in glioblastoma**. 2010, **17**(4):362–375.
19. Verhaak RG, Hoadley KA, Purdom E, Wang V, Qi Y, Wilkerson MD, Miller CR, Ding L, Golub T, Mesirov JP *et al*: **Integrated genomic analysis identifies clinically relevant subtypes of glioblastoma characterized by abnormalities in PDGFRA, IDH1, EGFR, and NF1**. Cancer Cell 2010, **17**(1):98–110.
20. Lathia J, Mack S, Mulkearns-Hubert E, Valentim C, Rich JJG, development: **Cancer stem cells in glioblastoma**. 2015, **29**(12):1203–1217.
21. Chen J, Li Y, Yu TS, McKay RM, Burns DK, Kernie SG, Parada LF: **A restricted cell population propagates glioblastoma growth after chemotherapy**. Nature 2012, **488**(7412):522–526.
22. Wang L, Babikir H, Müller S, Yagnik G, Shamardani K, Catalan F, Kohanbash G, Alvarado B, Di Lullo E, Kriegstein A *et al*: **The Phenotypes of Proliferating Glioblastoma Cells Reside on a Single Axis of Variation**. 2019, **9**(12):1708–1719.
23. Segerman A, Niklasson M, Haglund C, Bergström T, Jarvius M, Xie Y, Westermark A, Sönmez D, Hermansson A, Kastemar M *et al*: **Clonal Variation in Drug and Radiation Response among Glioma-Initiating Cells Is Linked to Proneural-Mesenchymal Transition**. 2016, **17**(11):2994–3009.
24. Zhang Z, Xu J, Chen Z, Wang H, Xue H, Yang C, Guo Q, Qi Y, Guo X, Qian M *et al*: **Transfer of MicroRNA via Macrophage-Derived Extracellular Vesicles Promotes Proneural-to-Mesenchymal Transition in Glioma Stem Cells**. Cancer Immunol Res 2020, **8**(7):966–981.
25. Johansson E, Grassi ES, Pantazopoulou V, Tong B, Lindgren D, Berg TJ, Pietras EJ, Axelson H, Pietras A: **CD44 Interacts with HIF-2alpha to Modulate the Hypoxic Phenotype of Perinecrotic and Perivascular Glioma Cells**. Cell Rep 2017, **20**(7):1641–1653.
26. Carro M, Lim W, Alvarez M, Bollo R, Zhao X, Snyder E, Sulman E, Anne S, Doetsch F, Colman H *et al*: **The transcriptional network for mesenchymal transformation of brain tumours**. 2010, **463**(7279):318–325.
27. Lau J, Ilkhanizadeh S, Wang S, Miroshnikova Y, Salvatierra N, Wong R, Schmidt C, Weaver V, Weiss W, Persson AJCr: **STAT3 Blockade Inhibits Radiation-Induced Malignant Progression in Glioma**. 2015, **75**(20):4302–4311.
28. Yang W, Soares J, Greninger P, Edelman E, Lightfoot H, Forbes S, Bindal N, Beare D, Smith J, Thompson I *et al*: **Genomics of Drug Sensitivity in Cancer (GDSC): a resource for therapeutic biomarker discovery in cancer cells**. 2013, **41**:D955-961.
29. Barretina J, Caponigro G, Stransky N, Venkatesan K, Margolin A, Kim S, Wilson C, Lehár J, Kryukov G, Sonkin D *et al*: **The Cancer Cell Line Encyclopedia enables predictive modelling of anticancer drug sensitivity**. 2012, **483**(7391):603–607.
30. Bindea G, Mlecnik B, Tosolini M, Kirilovsky A, Waldner M, Obenauf A, Angell H, Fredriksen T, Lafontaine L, Berger A *et al*: **Spatiotemporal dynamics of intratumoral immune cells reveal the immune landscape in human cancer**. 2013, **39**(4):782–795.

31. Gyori B, Venkatachalam G, Thiagarajan P, Hsu D, Clement MJRb: **OpenComet: an automated tool for comet assay image analysis**. 2014, **2**:457–465.
32. Podhorecka M, Skladanowski A, Bozko PJJona: **H2AX Phosphorylation: Its Role in DNA Damage Response and Cancer Therapy**. 2010, **2010**.
33. Fedele M, Cerchia L, Pegoraro S, Sgarra R, Manfioletti G: **Proneural-Mesenchymal Transition: Phenotypic Plasticity to Acquire Multitherapy Resistance in Glioblastoma**. Int J Mol Sci 2019, **20**(11).
34. Hegde A, Upadhya SJTin: **The ubiquitin-proteasome pathway in health and disease of the nervous system**. 2007, **30**(11):587–595.
35. Fu D, Lala-Tabbert N, Lee H, Wiper-Bergeron NJTJobc: **Mdm2 promotes myogenesis through the ubiquitination and degradation of CCAAT/enhancer-binding protein β**. 2015, **290**(16):10200–10207.
36. Lou J, Hao Y, Lin K, Lyu Y, Chen M, Wang H, Zou D, Jiang X, Wang R, Jin D *et al*: **Circular RNA CDR1as disrupts the p53/MDM2 complex to inhibit Gliomagenesis**. 2020, **19**(1):138.
37. Wagner E, Nebreda AJNrC: **Signal integration by JNK and p38 MAPK pathways in cancer development**. 2009, **9**(8):537–549.
38. Thornton T, Pedraza-Alva G, Deng B, Wood C, Aronshtam A, Clements J, Sabio G, Davis R, Matthews D, Doble B *et al*: **Phosphorylation by p38 MAPK as an alternative pathway for GSK3beta inactivation**. 2008, **320**(5876):667–670.
39. Prins N, Harrison J, Chu H, Blackburn K, Alam J, Scheltens P, JAsr, therapy: **A phase 2 double-blind placebo-controlled 24-week treatment clinical study of the p38 alpha kinase inhibitor neflamapimod in mild Alzheimer's disease**. 2021, **13**(1):106.
40. Duffy J, Harrington E, Salituro F, Cochran J, Green J, Gao H, Bemis G, Evindar G, Galullo V, Ford P *et al*: **The Discovery of VX-745: A Novel and Selective p38α Kinase Inhibitor**. 2011, **2**(10):758–763.
41. Goldsmith C, Kim S, Karunarathna N, Neuendorff N, Toussaint L, Earnest D, Bell-Pedersen DJBc: **Inhibition of p38 MAPK activity leads to cell type-specific effects on the molecular circadian clock and time-dependent reduction of glioma cell invasiveness**. 2018, **18**(1):43.
42. Su B, Chen JJM, biochemistry c: **Pharmacological inhibition of p38 potentiates antimicrobial peptide TP4-induced cell death in glioblastoma cells**. 2020, **464**:1–9.
43. Pegg A, Byers TJFjopotFoASfEB: **Repair of DNA containing O6-alkylguanine**. 1992, **6**(6):2302–2310.
44. Khan S, Bhat ZR, Jena G: **Role of autophagy and histone deacetylases in diabetic nephropathy: Current status and future perspectives**. Genes Dis 2016, **3**(3):211–219.
45. Brandner S, McAleenan A, Kelly C, Spiga F, Cheng H, Dawson S, Schmidt L, Faulkner C, Wragg C, Jefferies S *et al*: **MGMT promoter methylation testing to predict overall survival in people with glioblastoma treated with temozolomide: a comprehensive meta-analysis based on a Cochrane Systematic Review**. 2021, **23**(9):1457–1469.
46. Singh N, Miner A, Hennis L, Mittal SJCdr: **Mechanisms of temozolomide resistance in glioblastoma - a comprehensive review**. 2021, **4**:17–43.

47. Wu W, Klockow J, Zhang M, Lafortune F, Chang E, Jin L, Wu Y, Daldrup-Link HJPr: **Glioblastoma multiforme (GBM): An overview of current therapies and mechanisms of resistance**. 2021, **171**:105780.
48. Ohba S, Yamashiro K, Hirose YJC: **Inhibition of DNA Repair in Combination with Temozolomide or Dianhydrogalactiol Overcomes Temozolomide-Resistant Glioma Cells**. 2021, **13**(11).
49. Rominiyi O, Collis SJMo: **DDRugging glioblastoma: understanding and targeting the DNA damage response to improve future therapies**. 2021.
50. Sharifi Z, Abdulkarim B, Meehan B, Rak J, Daniel P, Schmitt J, Lauzon N, Eppert K, Duncan H, Petrecca K *et al*: **Mechanisms and Antitumor Activity of a Binary EGFR/DNA-Targeting Strategy Overcomes Resistance of Glioblastoma Stem Cells to Temozolomide**. 2019, **25**(24):7594–7608.
51. Garnier D, Meehan B, Kislinger T, Daniel P, Sinha A, Abdulkarim B, Nakano I, Rak JJN-o: **Divergent evolution of temozolomide resistance in glioblastoma stem cells is reflected in extracellular vesicles and coupled with radiosensitization**. 2018, **20**(2):236–248.
52. Wang X, Zhou R, Xiong Y, Zhou L, Yan X, Wang M, Li F, Xie C, Zhang Y, Huang Z *et al*: **Sequential fate-switches in stem-like cells drive the tumorigenic trajectory from human neural stem cells to malignant glioma**. 2021, **31**(6):684–702.
53. Verhaak R, Hoadley K, Purdom E, Wang V, Qi Y, Wilkerson M, Miller C, Ding L, Golub T, Mesirov J *et al*: **Integrated genomic analysis identifies clinically relevant subtypes of glioblastoma characterized by abnormalities in PDGFRA, IDH1, EGFR, and NF1**. 2010, **17**(1):98–110.
54. Patel A, Tirosh I, Trombetta J, Shalek A, Gillespie S, Wakimoto H, Cahill D, Nahed B, Curry W, Martuza R *et al*: **Single-cell RNA-seq highlights intratumoral heterogeneity in primary glioblastoma**. 2014, **344**(6190):1396–1401.
55. Galli R, Binda E, Orfanelli U, Cipelletti B, Gritti A, De Vitis S, Fiocco R, Foroni C, Dimeco F, Vescovi AJCr: **Isolation and characterization of tumorigenic, stem-like neural precursors from human glioblastoma**. 2004, **64**(19):7011–7021.
56. Wang Q, Hu B, Hu X, Kim H, Squatrito M, Scarpace L, deCarvalho A, Lyu S, Li P, Li Y *et al*: **Tumor Evolution of Glioma-Intrinsic Gene Expression Subtypes Associates with Immunological Changes in the Microenvironment**. 2018, **33**(1):152.
57. Wang S, Qi Y, Gao X, Qiu W, Liu Q, Guo X, Qian M, Chen Z, Zhang Z, Wang H *et al*: **Hypoxia-induced lncRNA PDIA3P1 promotes mesenchymal transition via sponging of miR-124-3p in glioma**. 2020, **11**(3):168.
58. Xie C, Zhang L, Chen Z, Zhong W, Fang J, Zhu Y, Xiao M, Guo Z, Zhao N, He X *et al*: **A hMTR4-PDIA3P1-miR-125/124-TRAF6 Regulatory Axis and Its Function in NF kappa B Signaling and Chemoresistance**. 2020, **71**(5):1660–1677.
59. Sun C, Zhang L, Li G, Li S, Chen Z, Fu Y, Gong F, Bai T, Zhang D, Wu Q *et al*: **The lncRNA PDIA3P Interacts with miR-185-5p to Modulate Oral Squamous Cell Carcinoma Progression by Targeting Cyclin D2**. 2017, **9**:100–110.

60. Humphreys L, Smith P, Chen Z, Fouad S, D'Angiolella VJCd, differentiation: **The role of E3 ubiquitin ligases in the development and progression of glioblastoma**. 2021, **28**(2):522–537.
61. Fu D, Lala-Tabbert N, Lee H, Wiper-Bergeron N: **Mdm2 promotes myogenesis through the ubiquitination and degradation of CCAAT/enhancer-binding protein beta**. J Biol Chem 2015, **290**(16):10200–10207.
62. Weston C, Lambright D, Davis RJS: **Signal transduction. MAP kinase signaling specificity**. 2002, **296**(5577):2345–2347.
63. Filippi-Chiela E, Bueno e Silva M, Thomé M, Lenz GJA: **Single-cell analysis challenges the connection between autophagy and senescence induced by DNA damage**. 2015, **11**(7):1099–1113.
64. Hirose Y, Katayama M, Mirzoeva O, Berger M, Pieper RJCr: **Akt activation suppresses Chk2-mediated, methylating agent-induced G2 arrest and protects from temozolomide-induced mitotic catastrophe and cellular senescence**. 2005, **65**(11):4861–4869.
65. Patil C, Nuño M, Elramsisy A, Mukherjee D, Carico C, Dantis J, Hu J, Yu J, Fan X, Black K *et al*: **High levels of phosphorylated MAP kinase are associated with poor survival among patients with glioblastoma during the temozolomide era**. 2013, **15**(1):104–111.
66. Ghosh D, Nandi S, Bhattacharjee SJC, medicine t: **Combination therapy to checkmate Glioblastoma: clinical challenges and advances**. 2018, **7**(1):33.
67. Silber J, Bobola M, Blank A, Schoeler K, Haroldson P, Huynh M, Kolstoe DJCcraojotAAfCR: **The apurinic/apyrimidinic endonuclease activity of Ape1/Ref-1 contributes to human glioma cell resistance to alkylating agents and is elevated by oxidative stress**. 2002, **8**(9):3008–3018.

Figures

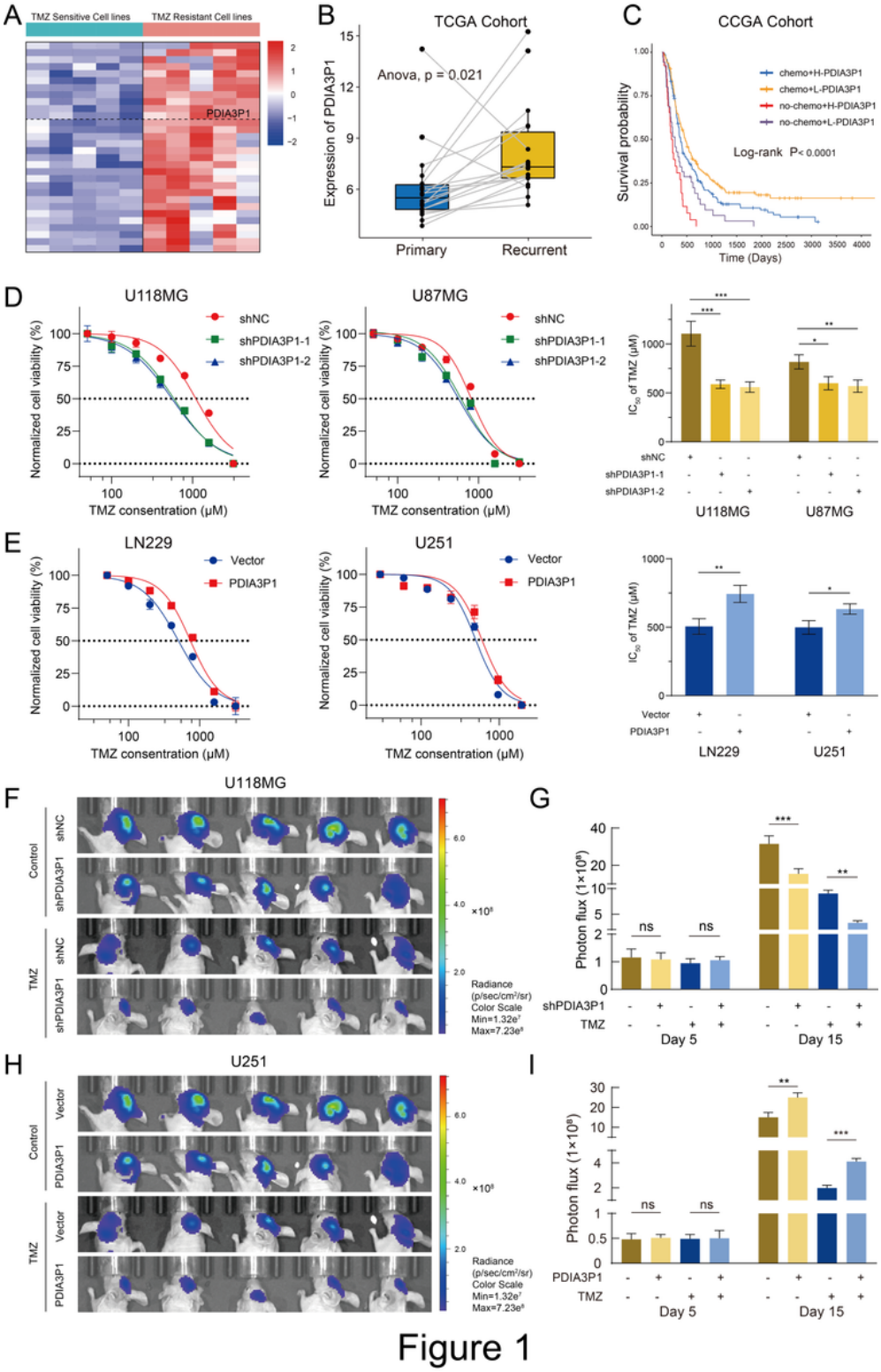

Figure 1

Figure 1

PDIA3P1 is markedly upregulated in TMZ-resistant cell lines and promotes TMZ resistance.

A Heatmap showed that PDIA3P1 was upregulated in TMZ resistance cell lines. B The expression of PDIA3P1 is higher in primary gliomas than in recurrent gliomas. C Survival analysis of GBM patients stratified by whether they received chemotherapy and expression level of PDIA3P1. D Cell viability assay

of PDIA3P1-knockdown and control U118MG and U87MG cells treated with various concentrations of TMZ for 48h. The detailed IC50 were listed in the right panel. E Cell viability assay of PDIA3P1-overexpression and control LN229 and U251 cells treated with various concentrations of TMZ for 48h. The detailed IC50 were listed in the right panel. F H Bioluminescence imaging of tumor growth in xenograft nude mice with PDIA3P1 knockdown (F) or overexpression (H) and receiving or exempt from TMZ treatment in U118MG and U251 xenografts, respectively. G I The quantification of the photon counts of U118MG and U251 xenografts, respectively. The tumor sizes were monitored on day 5 and day 21.

Figure 2

Knockdown of PDIA3P1 exacerbates DNA damage and proliferation inhibition induced by TMZ intervention.

A B Representative images and quantification of Comet assay showing the DNA damage caused by PDIA3P1 knockdown or vehicle control with or without TMZ treatment (400μM, 48h) on U118MG (A) and U87MG (B) cells. Scale bars, 100μm. C D Representative images and quantification of γ-H2AX staining on U118MG (C) and U87MG (D) cells with or without TMZ treatment (400μM, 48h). Scale bars, 10μm. E Representative images of U118MG cells subjected to the EdU cell proliferation assay (upper panel; scale bar, 200 μm) and quantification of EdU-positive cells (lower panel) with or without TMZ treatment (400μM, 48h). F Apoptosis assay showing the effect of PDIA3P1 knockdown on U118MG with or without TMZ treatment (400μM, 48h). The lower panel was the quantification of apoptosis cells.

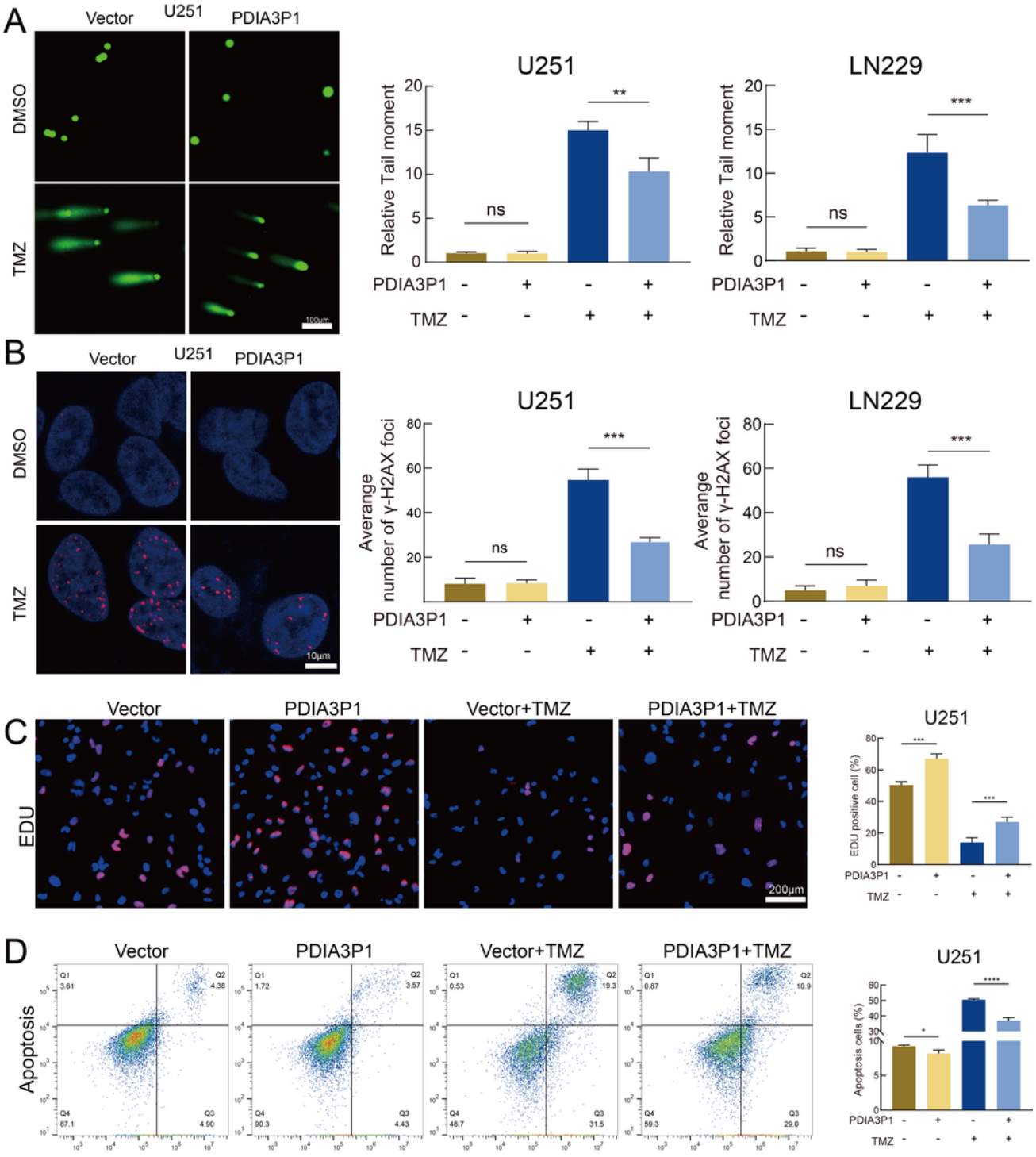

Figure 3

Figure 3

Overexpression of PDIA3P1 counteracted TMZ treatment-induced DNA damage and growth inhibition.

A Representative images and quantification of Comet assay on ov-PDIA3P1 or Vector U251 and LN229 cells with or without TMZ treatment (400μM, 48h). Scale bar, 100μm. B Representative images and quantification of γ-H2AX staining on ov-PDIA3P1 or Vector U251 and LN229 cells with or without TMZ

treatment (400μM, 48h). Scale bar, 10μm. C Representative images of U251 cells subjected to the EdU cell proliferation assay (left panel; scale bar, 200μm) and quantification of EdU-positive cells (right panel) with or without TMZ treatment (400μM, 48h). D Apoptosis assay showing the effect of PDIA3P1 overexpression on U251 with or without TMZ treatment (400μM, 48h). The right panel was the quantification of apoptosis cells.

Figure 4

Elevated expression of PDIA3P1 is associated with Mesenchymal subtype.

A Statistical analysis of PDIA3P1 in normal, proneural and mesenchymal tissues in the TCGA GBM dataset. B The relative expression of PDIA3P1 in NPC, PN GSCs and MES GSCs. C ROC curves of PDIA3P1 for MES-GBM subtype prediction in TCGA. D The PDIA3P1 expression is negatively correlated with PN related genes and positively correlated with MES related genes. E GSEA showed a significant positive correlation between high expression of PDIA3P1 and MES subtypes, and a negative correlation with PN subtypes. F Representative images of IF staining revealing the effect of PDIA3P1 knockdown on the expression of CD44 and SOX2 in GSC20 and GSC267, respectively. scale bar, 10μm. G Extreme limit dilution assays showing a decreased self-renewal ability after knockdown of PDIA3P1 in GSC20 and GSC267, respectively. H The protein expression of MES markers after PDIA3P1 knockdown in GSC20 and GSC267.

Figure 5

PDIA3P1 stabilizes C/EBPβ by preventing MDM2 -mediated ubiquitination.

A Different protein bands pulled down by PDIA3P1 junction sense or anti-sense in GSC267 cells. B RNA pull down assay showing the interaction between C/EBPβ with PDIA3P1. C RIP and qRT-PCR assays revealing the interaction between C/EBPβ with PDIA3P1. D The protein expression effected by PDIA3P1 knockdown and C/EBPβ overexpression. E F Overexpression of C/EBPβ rescued the effect of PDIA3P1 knockdown on self-renewal ability of GSC267. Scale bar, 200μm. G H Knockdown of C/EBPβ inhibited the effect of PDIA3P1 overexpression on self-renewal ability of GSC8-11. Scale bar, 200μm. I Quantification of comet assay and γ-H2AX staining of GSC267 under TMZ treatment (400μM, 48 h). J Quantification of comet assay and γ-H2AX staining of GSC8-11 under TMZ treatment (400μM, 48 h). K Western blotting analysis of the effect of PDIA3P1 knockdown on C/EBPβ with or without MG132 treatment (10μM, 12h). L Western blotting analysis of C/EBPβ in PDIA3P1 stable knockdown and control GSC267 cells after treatment with CHX (100 μg/ml) for indicated times. M GSCs lysates were immunoprecipitated with anti-C/EBPβ antibody followed by immunoblotting with anti-Ubiquitin antibody and anti-C/EBPβ antibody.

The GSCs were pretreated with MG132 (10μM) for 6 hours. N Co-IP analysis of interaction between C/EBPβ and MDM2 in GSC267 cells transfected with PDIA3P1 or shPDIA3P1.

Figure 6

PDIA3P1 is upregulated in response to TMZ-induced activation of the p38-MAPK signaling pathway.

A B PDIA3P1 expression was induced by TMZ treatment in a dose-dependent (treatment with different concentrations of TMZ for 48 hours) and time-dependent (treatment with 400μM TMZ for indicated times) manner. C Bubble plot visualized the significantly enriched GO biological pathways using genes upregulated in TMZ-treated GSC group in GSC68029. C Cell viability assay in GSC20, GSC267, U118MG, and U251 treated with different concentrations of NEF for 48 h. E NEF treatment (50μM, 48h) abrogated elevation of PDIA3P1 expression induced by TMZ treatment. F Cells were treated with TMZ in combination with NEF at different concentrations and percentages of growth inhibition were visualized. G CI scores of cells treated with TMZ in combination with NEF at different concentrations. H Pearson correlation test was performed to show the correlation of PDIA3P1 expression with JUN in TCGA and CGGA datasets, respectively. I Knocking down of JUN expression using siRNA reduced the expression of PDIA3P1 (left panel). Knocking down of JUN counteracted TMZ treatment (400μM, 48h) induced upregulation of PDIA3P1 (right panel). J The recognition motif of JUN obtained from the JASPAR (upper panel) and schematic illustration of four fragments in promoter sequence of PDIA3P1 (lower panel). K The luciferase assay showed PDIA3P1 knockdown reduced promoter activity in fragments 1-3. L ChIP-PCR assay showed that JUN bound to a predicted site within the PDIA3P1 promoter.

Figure 7

NEF combined with TMZ confers a better anti-tumor effect both in vitro and in vivo.

A B The representative images (A) and quantification (B) of comet assay showed that TMZ (400μM, 48h) combined with NEF (50μM, 48h) contributed a stronger DNA damage effect in GSC20 and GSC267, respectively. scale bar, 100μm. C D The representative images (C) and quantification (D) of γ-H2AX staining in GSC20 and GSC267 (TMZ 400μM, 48h. NEF 50μM, 48h). Scale bar, 10μm. E F Representative images of IF staining showed the effect of NEF treatment (50μM, 48h) and PDIA3P1 overexpression on the expression of CD44 and SOX2 in GSC20 (E) and GSC267 (F), respectively. scale bar, 10μm. G Bioluminescence imaging (upper panel) and quantification (lower panel) of tumor size in GSC267 xenografted nude mice treated with PBS, NEF (5mg/kg, p.o., 5 days per week), TMZ (5mg/kg, p.o., 5 days per week) or both drugs in combination. H Working model plot showing that PDIA3P1 plays a key role in promoting the TMZ resistance of GBM cells. The p38α-JUN was activated by TMZ treatment and promoting the transcription of PDIA3P1. PDIA3P1 disrupted the MDM2-C/EBPβ complex to stabilize

C/EBPβ and promote PN-MES transition, thereby promoting the resistance of GBM cells to TMZ treatment. NEF, a highly selective p38α inhibitor, inhibited TMZ-induced upregulation of PDIA3P1 expression and provided a promising strategy to address the challenge of TMZ resistance in glioma cells.

Supplementary Files

This is a list of supplementary files associated with this preprint. Click to download.

- SupplementaryFigures.docx
- table.xlsx